Fracture process zone characteristics and identification of the micro-fracture phases in recycled concrete

Menghuan Guo, Syed Yasir Alam, Ahmed Zakarya Bendimerad, Frédéric Grondin, Emmanuel Rozière, Ahmed Loukili

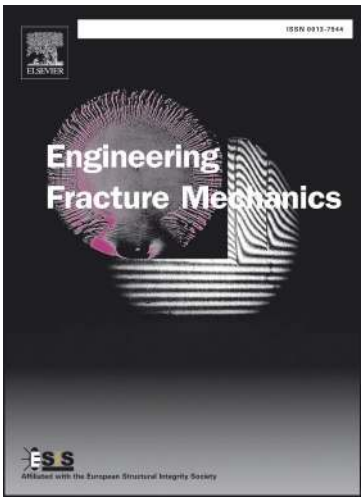

Fracture process zone characteristics and identification of the micro-fracture phases in recycled concrete

Menghuan Guo, Syed Yasir Alam, Ahmed Zakarya Bendimerad, Frédéric Grondin, Emmanuel Rozière, Ahmed Loukili

PII: S0013-7944(17)30406-X
DOI: http://dx.doi.org/10.1016/j.engfracmech.2017.07.004
Reference: EFM 5606

To appear in: *Engineering Fracture Mechanics*

Received Date: 20 April 2017
Revised Date: 3 July 2017
Accepted Date: 3 July 2017

Please cite this article as: Guo, M., Alam, S.Y., Bendimerad, A.Z., Grondin, F., Rozière, E., Loukili, A., Fracture process zone characteristics and identification of the micro-fracture phases in recycled concrete, *Engineering Fracture Mechanics* (2017), doi: http://dx.doi.org/10.1016/j.engfracmech.2017.07.004

Fracture process zone characteristics and identification of the micro-fracture phases in recycled concrete

Menghuan Guo, Syed Yasir Alam, Ahmed Zakarya Bendimerad,

Frédéric Grondin, Emmanuel Rozière, Ahmed Loukili

Institut de Recherche en Génie Civil et Mécanique (GeM), UMR-CNRS 6183, Centrale Nantes, Université de Nantes, 1 rue de la Noë, 44321 Nantes, France – e-mail: {menghuan.guo ; syed-yasir.alam ; ahmed.bendimerad ; frederic.grondin ; emmanuel.roziere ; ahmed.loukili} @ec-nantes.fr

Abstract

Normal and recycled aggregate concrete differ significantly in their fracture characteristics. The cracking in recycled concrete initiates earlier; the fracture length is generally larger and the use of high proportion of recycled aggregate results in higher strain gradients in the fracture process zone. However, in spite of the negative influences, the mechanical responses of normal concrete and concrete with 30% recycled aggregate are similar to each other. This paper shows the influence of recycled aggregate proportion on the characteristics of fracture process. Furthermore, classification of the recorded acoustic signals during the fracture test was carried out; three clusters correspond respectively to aggregate fracture, cracking in cement mortar and cracking at the interfacial transition zone were discriminated. The evolution of each micro-fracture phase in terms of the mechanical state of the material was analyzed. A comparison of the apparition chronology of each cluster for normal concrete and recycled concrete was carried out.

Keywords: recycled aggregate; digital image correlation; acoustic emission; fracture; cluster analysis

Nomenclature

AE	acoustic emission
CMOD	crack mouth opening displacement
CTOD	crack tip opening displacement
DIC	digital image correlation
E_{dyn}	dynamic elastic modulus
FPZ	fracture process zone
f_{c28}	compressive strength at 28 days
f_{tsp28}	splitting tensile strength at 28 days
G_f	fracture energy
ITZ	interfacial transition zone
l_{ch}	characteristic length
PCA	principle component analysis
RAC	recycled aggregate concrete
SLZ	strain localization zone
UWC	unknown waste concrete
WA_{24}	water absorption at 24h

1. Introduction

With the growing waste disposal crisis and depletion of natural construction materials, the use of recycled aggregate concrete (RAC) has been advocated in the past three decades. The standard NF EN 206-1/CN 2014 [1] has authorized the maximum replacement percentage of recycled aggregate according to the aggregate type and the exposure class. Previous research has shown that RAC is composed of natural aggregate, recycled aggregate, old and new interfacial transition zones (ITZs), and

cement mortar [2]; [3]; [4]. Generally, previous cracks exist in recycled aggregate; a layer of old residual mortar is attached around the aggregate particles [5]. These features lead to higher water absorption, lower density and lower particle strength of recycled aggregate [6]; [7]; [8]. Moreover, a porous microstructure consisting of voids and calcium hydroxide has been found for the two types of ITZ [9]; [10]. The characteristics of recycled aggregate and ITZ can highly influence the mechanical properties of RAC [9]; [11]; [12]; [13], which are generally inferior to those of normal concrete [14]; [15]; [16]. However, some researchers [8]; [14]; [17] have observed that the global failure behavior of RAC specimens under compression, tension or flexion is similar to that of conventional concrete specimens respectively. Furthermore, the performance evaluation of a concrete mix is not only limited to the determination of its conventional mechanical properties since it is of practical significance to characterize the fracture process of a quasi-brittle material [17]; [18]. Among the fracture characteristics of a concrete mix, the crack length and width developments are the most important features [20]; [21]; [22]. Thus, a quantitative analysis of the fracture process of RAC and a thorough understanding of its potential load carrying capacity are highly needed.

Li et al. [23] have investigated the fracture process of RAC by testing the specimens with artificial recycled aggregate distribution; the cracks in RAC are found to appear around both the old and new ITZs, and then propagate into the mortar matrix. The initiation and propagation of microcracks are different between RAC and normal concrete. However, little work has been found to inspect the crack propagation process in a given actual recycled concrete specimen. Besides, the fracture process of concrete is also reflected in the growth of strain localization zone [24], the identification of which is also beneficial for the understanding of the failure process of RAC.

The aim of this work is to show that the existing traditional approaches such as the comparison of fracture properties (characteristic length l_{ch} and fracture energy G_f) of concrete are not sufficient to characterize the material. Although the experimental techniques to determine the fracture properties of concrete have been extensively studied [25]; [26]; few of them provide the possibility to identify the micro-mechanisms linked to each phase of the microstructure. The originality of this study is to develop one approach for analyzing quantitatively the micro-fracture in each phase of the material and studying the roles of the different phases on the failure behavior of the heterogeneous recycled material. This approach can also be used to investigate the evolution of each kind of micro-fracture in terms of the mechanical state of the material at the mesoscopic scale.

Acoustic emission (AE) is a well-established technique for the characterization of fracture process. It has been used mainly to identify the fracture mechanisms by recording energy dissipation process using AE technique, for instance [20]; [27]; [28]; [29]; [30]. AE is also used to define the boundary of the fracture process zone (FPZ) and the energy dissipation zone in order to relate it with characteristic length of the material [20]; [29]. The distribution of energy release during the fracturing process along the length and width of FPZ has been analyzed using AE sources and energy histograms [31]; [32]; [33]; [34]. Classification of cracks has also been performed using different AE parameters like the average frequency, RA, energy [35]; [36] and moment tensor analysis [35].

AE technique characterizes the cracks when energy dissipation process is active, irrespective of the crack opening process [37]. The later can be efficiently measured by digital image correlation (DIC) technique. Such methods require recording displacement fields and mapping strain localization zone [24]; [38]; [39]; [40]; [41]. The size and

intensity of the fracture are estimated based on strain values or by calculating crack openings from displacement field. Based on the discontinuous displacement field near the propagating crack, various crack characteristics such as crack openings, crack length and strain profiles can be extracted with post processing procedures and finite element shape functions [40]; [42].

This study attempts to provide insights into the failure mechanism of recycled concrete beams under three-point bending tests by applying simultaneously the DIC and AE techniques. The combination of the two methods gives the possibility of comparing different kinds of concrete that exhibit very similar global mechanical properties but have distinctive microcracking characteristics. In order to interpret the brittleness of recycled concrete, it is very interesting to propose one methodology for identifying the different microcracking phases in the material. To achieve this, a multi-parametric clustering analysis of the captured AE signals was conducted; the damage mechanisms of RAC can thus be identified and the corresponding signal sources can be discriminated.

2. Material properties

This study is part of the French national projects RECYBETON [43] and ECOREB [44], where the task of defining the mixture proportions was done by other partners [7]; [16]; [45]; [46]. The mixtures have been established by the software BETONLAB [47]: (1) the granular skeleton was optimized at first for the minimization of the clamping index; this sets the optimum quantities of sand and aggregate (2) the water, cement and superplasticizer contents have been adjusted to achieve the desired slump and strength while minimizing the cost. In this way, the W/C ratio has been chosen to be 0.65, which is the acceptable maximum value for dry or permanently wet environment (XC1) according to standard NF EN 206-1/CN 2014 [1]. Concrete mixtures were prepared

with CEM II/A-L 42.5N, crushed limestone aggregate, and recycled aggregate. Recycled aggregate was obtained by crushing of unknown waste concrete. The fine aggregate used is crushed fine sand, which has a maximum size not greater than 4 mm. The corresponding properties of coarse and fine aggregate are shown in Table 1. The limestone filler Betocarb HP OG was added in all the mixtures so as to improve the granular skeleton; also the W/C ratio was slightly adjusted in the three mixes in order to achieve similar overall properties. All aggregates used in concrete mixtures were at saturated surface-dried state so as to eliminate the effect of dissimilar water absorption in natural and recycled aggregate. Variation of the percentage of recycled aggregate (0, 30% and 100%) vis-à-vis total mass of coarse aggregate in concrete mixtures has been studied. The mixtures were designed so as to have the same compressive strength in the range of 25-30 MPa and the same workability according to the structural class S4 [48]. Table 2 shows the quantities of constituent materials of the mix design for three types of concrete: C-N-N: Concrete with Natural sand and Natural aggregate; C-N-30R: Concrete with Natural sand and 30% Recycled aggregate; C-N-100R: Concrete with Natural sand and 100% Recycled aggregate.

Table 1: Properties of aggregate (WA_{24} = water absorption at 24h; UWC = Unknown waste concrete).

	Natural aggregate			Recycled aggregate	
	Sand 0/4 mm	Aggregate 4/10 mm	Aggregate 6.3/20 mm	Aggregate 4/10 mm	aggregate 10/20 mm
Mineralogy	Sandrancourt Sand	Dark limestone	Dark limestone	UWC	UWC
WA_{24} (%)	1.2	0.56	0.53	5.3	4.89
Density(kg/m^3)	2.6	2.73	2.73	2.34	2.32

The mechanical properties of concrete were determined at 28 days on $\phi 110 \times 220$ mm^2 cylinders and the results (Table 3) are the average values of two specimens. It shows

clearly that use of 100% recycled aggregate lowers the compressive strength by 10% and the tensile strength by 3% compared to normal concrete.

Table 2: Concrete mix proportions.

Concrete	C-N-N	C-N-30R	C-N-100R
W/C ratio	0.64	0.65	0.65
Water (kg/ m^3)	180	185	189
Cement (kg/ m^3)	270	276	282
Sand 0/4 mm (kg/ m^3)	780	813	806
Aggregate 6.3/20 mm (kg/ m^3)	820	462	-
Aggregate 4/10 mm (kg/ m^3)	267	228	-
Recycled Aggregate 10/20 mm (kg/	-	296	701
Recycled Aggregate 4/10 mm (kg/	-	-	163
Limestone filler (kg/ m^3)	45	31	31
Superplasticizer (kg/ m^3)	1.31	1.51	1.4
Slump (cm)	20	20	20

Table 3: Mechanical properties of concrete.

Concrete	f_{c28} (MPa)	f_{tsp28} (MPa)	E_{dyn} (GPa)
C-N-N	28.1±3.2	2.48±0.03	40.9±0.3
C-N-30R	26.7±2.7	2.46±0.02	37.4±0.8
C-N-100R	25.2±0.3	2.40±0.01	33.1±0.5

3. Experimental methods

For the flexural test, 100 × 200 × 800 mm^3 (width×height×length) concrete beams were prepared with an effective span equals to 600 mm. The beams were notched at midspan with a notch depth of 40 mm. The fracture test of the specimens at the age of 28 days was carried out using a universal testing machine as per RILEM-TMC50 recommendations with the loading cell capacity of 160 kN and servo-hydraulic regulation. The load was controlled by crack mouth opening displacement (CMOD) rate of 0.2 µm/s. During the test, the crosshead displacement was also recorded. Minimum

number of three beams for each class was tested to study the variation of experimental results.

Images of resolution 2452 × 2056 pixels were acquired at the rate of one image per second during the load test and a digital camera with 50 mm macro lens was used to capture images of the beam. The camera was mounted in order to image an area of approximately 110 × 160 mm^2 above the notch of the beam. The correlation of the stored digital images was performed with a commercial package Vic-2D by calculating the deformation between the reference image and a deformed image.

The device for the acquisition and signal processing of AE is consisted of a data acquisition system MISTRAS 8 channels. Eight piezoelectric transducers with a frequency of 50-200 kHz and a resonance frequency of 150 kHz were placed on the beam around the expected location of FPZ. They form a parallelogram position (12 × 12 cm^2) on each side of the specimen. The recorded AE signals were amplified by a 40 dB gain differential amplifier. A detection limit of 35 dB was chosen to overcome the background noise. The propagation velocity and the attenuation of acoustic waves were also measured. The wave propagation velocity was 4400 m/s for normal concrete and 4000 m/s for recycled concrete. In order to eliminate mechanical and electro-magnetic disturbances, a high pass filter with a cut-off frequency of 20 kHz, and a low-pass filter with a cut-off frequency of 400 kHz were used. Each waveform was digitized and stored with AEwin® system. The descriptors were further analyzed and evaluated with Noesis® software. A general view of the experimental setup is provided in Figure 1.

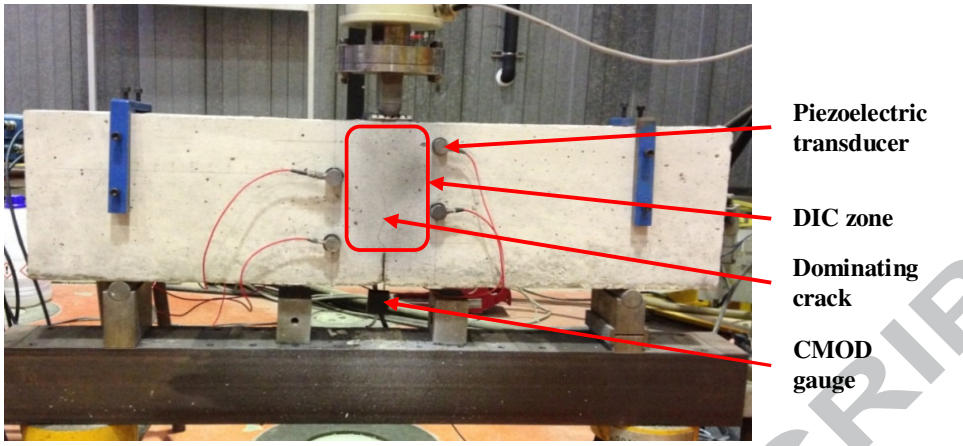

Figure 1: Experimental setup.

4. Results and discussion

4.1 Influence on global fracture properties

The average load-CMOD curves for the three kinds of concrete are presented in Figure 2. We can observe that the pre-peak response is almost identical for normal concrete and recycled concrete. While after peak a steeper softening branch is observed in recycled concrete, which illustrate the reduction of crack meandering during the failure of recycled concrete.

The characteristic fracture properties of concrete were calculated using experimental load-deflection curves. According to the RILEM work of fracture method [49]; [50], the fracture energy (G_f [J/m^2]) is determined by taking the ratio of the total energy consumed during fracture (W_f [N*m]) to the area of the initially uncracked ligament (A_{lig} [m^2]):

$$G_f = \frac{W_f}{A_{lig}} = \frac{W_0 + mg\delta_0}{b(d - a_0)}$$

W_f is divided into the work dissipated in the area under the load-deflection curve (W_0 [N*m]) and the maximum displacement (δ_0[m]) weighted by the mass of the specimen between the supports (mg [N]).

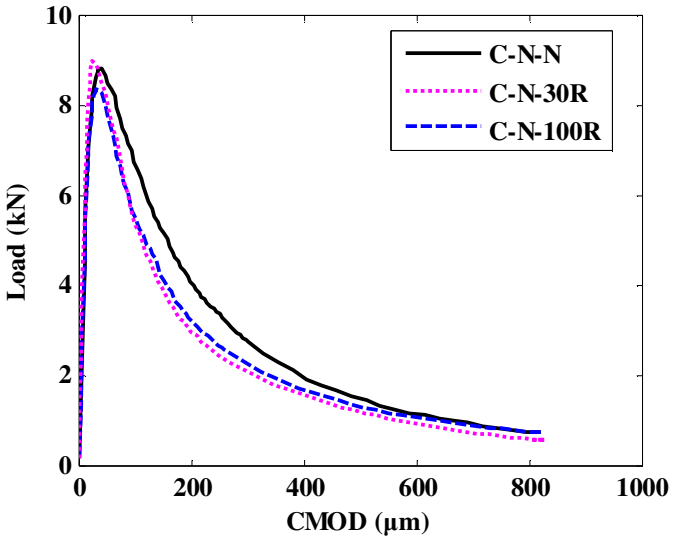

Figure 2: Average Load-CMOD curves for beams C-N-N, C-N-30R and C-N-100R

The material characteristic length (l_{ch} [mm]) is a principal material fracture property. It is directly related to the material brittleness and is proportional to the size of the FPZ according to Hillerborg [21]. It is determined by the following relation:

$$l_{ch} = \frac{E G_f}{f_t^2}$$

The corresponding results are summarized in Table 4. Note again that the fracture energy of recycled concrete is lower than that of natural aggregate concrete though all the three kinds of concrete have the same designed strength range. Accordingly, the characteristic length of recycled material reduces as the recycled aggregate content increases. A significant decrease in G_f can also be observed in Table 4. The value of G_f decreases up to 18% and for l_{ch} the decrease is 30%. This phenomenon coincides with the previous studies [8] that the reductions of G_f and l_{ch} are higher than those measured in compressive or tensile strength. Furthermore, according to Karihaloo [51], the l_{ch} captures the intrinsic ductility of the concrete mix and the larger the l_{ch} the more ductile the concrete mix, which is consistent with our analysis. However, it should be pointed out that the global mechanical behaviors of the three kinds of concrete are similar; the

impact of recycled aggregate upon the failure mechanism of material needs to be checked more closely with the DIC method.

Table 4: Fracture properties of concrete.

Concrete	G_f (J/ m^2)	l_{ch} (mm)
C-N-N	107.5±11.0	714.9±58.0
C-N-30R	95.6±7.0	586.1±45
C-N-100R	88.3±9.0	507.4±55

4.2 Analysis of the fracture process zone size characteristics

4.2.1. Crack development

The crack opening profiles (from the notch tip) along the height of beam are calculated for four levels of loading (80% pre-peak, 90% pre-peak, peak and 90% post-peak) and the results are demonstrated in Figure 3. We can see that the crack opening varies almost linearly along the height of the specimen until the closure of crack i.e. when the measured crack opening becomes zero. The crack openings develop with the increasing load and the maximum rate is observed around the peak load for all beams. However, there are significant differences among the three kinds of concrete. It is noteworthy that for C-N-100R, crack opening initiates earlier and faster than other concrete.

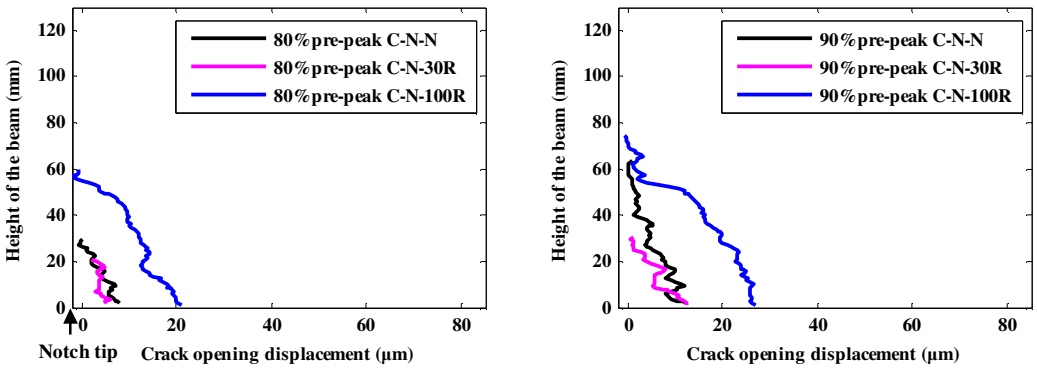

(a) (b)

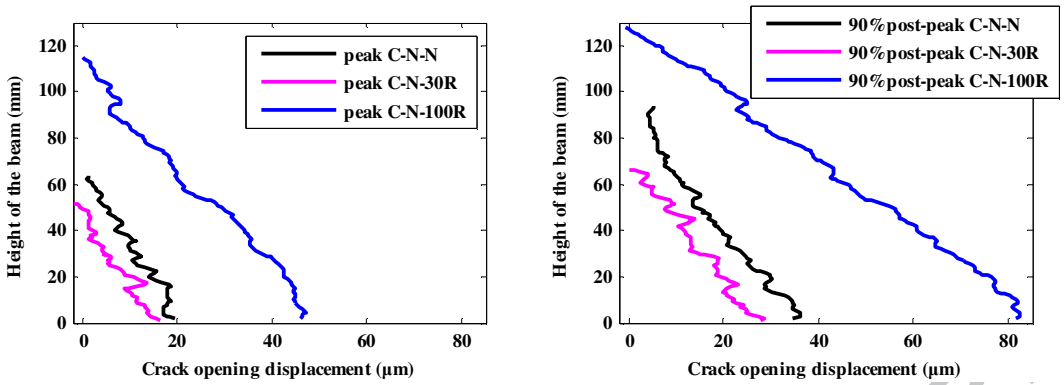

(c) (d)

Figure 3: Crack opening profiles at (a) 80% pre-peak; (b) 90% pre-peak; (c) peak; (d) 90% post-peak loading steps.

4.2.1.1. Evolution of crack length

Based on the crack opening profiles, the FPZ length (measured from the notch tip) can be approximately determined by measuring the cracking zone. Actually, the crack tip is "blurred" by microcracks in the FPZ [20]; therefore, the fracture zone length measured in this work is the length of the cumulative crack opening zone where the crack is still open [52]. The corresponding results for the three types of concrete are presented in Figure 4.

It is observed that for the three types of concrete the cracks initiate before the peak load and develop fast until 90% post-peak. Then, the increase slows down. The development of fracture process can be divided into three stages. The first stage for C-N-N, C-N-30R and C-N-100R is situated between the crack initiation and the 90% pre-peak loading. Within this stage, the crack growth is smooth. For C-N-100R, the crack formation starts from the 60% pre-peak loading step; for C-N-30R, it begins at 70% pre-peak loading step; and for C-N-N there are no apparent cracks until 80% pre-peak loading step. The cracking of C-N-100R increases at the highest rate and its fracture length is two times longer than that of C-N-N. Moreover, the initial fracture lengths for C-N-100R and C-N-30R are also larger. These differences may be explained by the relative porous

microstructure of RAC and also by the large amount of pre-existed cracks in recycled aggregate. For the second stage from 90% pre-peak to 90% post-peak, the crack grows much faster, especially for C-N-100R. The fracture length of the later is always larger than that of C-N-N, while for C-N-30R the opposite case is observed. At the end of this stage i.e. 90% post-peak loading step, the fracture length of C-N-100R reaches almost 80% of its final length, whereas for C-N-N it takes up only 55%. We can conclude that more the recycled aggregate content increases, more the cracking of concrete develops earlier and faster. During the last stage, the cracks in C-N-N, C-N-30R and C-N-100R increase gradually. The final crack lengths (at 20% post-peak loading step) of C-N-30R and C-N-100R are respectively 10 mm less and 10 mm more than that of C-N-N.

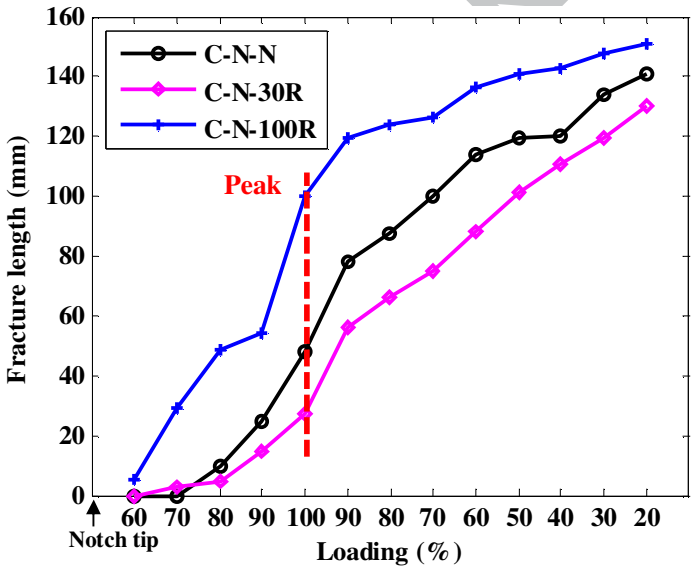

Figure 4: Development of the fracture length for beams C-N-N, C-N-30R and C-N-100R during loading.

Furthermore, after the rupture we have noticed that there were more crushed coarse aggregate rather than the deboned coarse aggregate on the fracture surface of beam C-N-100R, which is in accordance with the lower particle strength of recycled aggregate. The fracture surface of C-N-N is much more tortuous and the cracks are more likely to pass by the natural aggregate, while in C-N-100R the cracks tend to pass through the

recycled aggregate. This phenomenon explains well the less branching of cracks during the failure of recycled concrete and makes it evident that the values of G_f and l_{ch} of recycled concrete decrease due to the addition of recycled aggregate. Moreover, the trans-aggregate fracture can result in a lower interlocking strength and limit the concrete contribution when applying shear stress on the reinforced recycled concrete structure.

4.2.1.2. Evolution of crack tip opening displacement

The crack tip opening displacement (CTOD) for each beam is also calculated by evaluating the width of the displacement jump zone just above the notch tip during the whole loading steps (Figure 5). The feature of CTOD evolution is similar to that of the fracture length evolution for the three kinds of concrete. It is remarked that the incorporation of 30% recycled aggregate has very limited impact on the CTOD development. While for C-N-100R, the CTOD develops faster and its value is the highest compared to other concrete; at the maximum loading step, it reaches almost 50 µm. According to Wang et al. [53], when a specimen is loaded to have a crack opening displacement smaller than 50 µm prior to unloading, the crack opening has little effect on concrete permeability. It is only when the crack opening displacement exceeds 50 µm, the concrete permeability may rise substantially. In this case, the CTOD before peak is still within the limit.

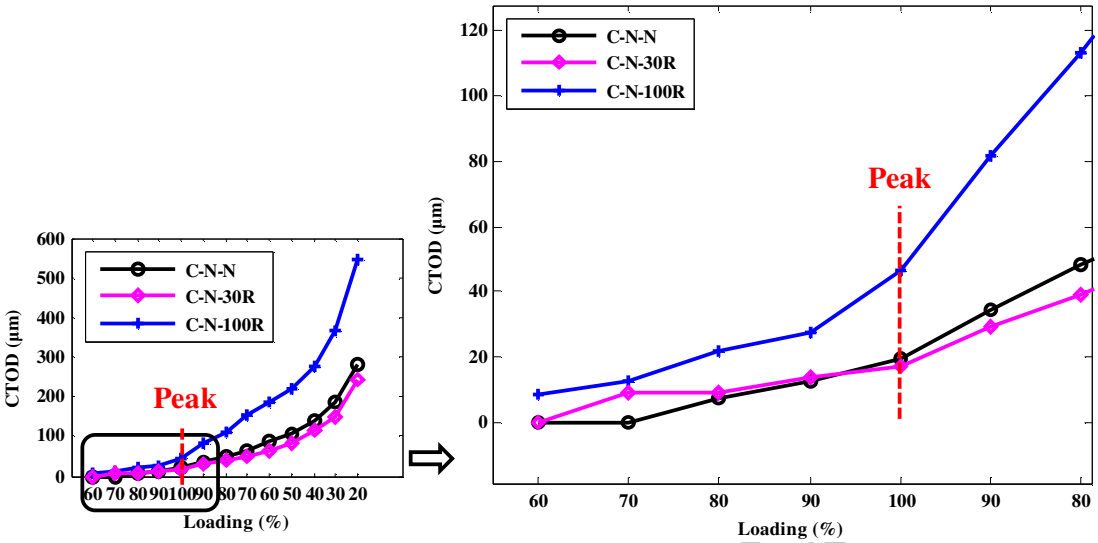

Figure 5: Development of the CTOD for beams C-N-N, C-N-30R and C-N-100R during loading.

4.2.2. Evolution of the width of the strain localized damaged zone

During loading, the microcracks first appear and then change gradually into dominant distinct macroscopic discrete cracks up to failure, as obviously shown in Figure 3. This fracture process is also reflected in the strain development. In fact, we have identified the strain localization zone (SLZ), the central part of FPZ, for the three types of concrete by image processing. Only the strain in X-direction (ε_{xx}) is provided; because the strain in Y-direction ε_{yy} and the shear strain ε_{xy} are significantly (5-10 times) smaller [41]. Nevertheless, the strain pattern is obtained using continuum mechanics laws. Consequently, only the strains before the appearance of a macrocrack are meaningful. The comparison for the three kinds of concrete at peak load is illustrated in Figure 6. The strain value of C-N-100R is the highest and the length of the SLZ is the largest compared to other concrete. The influence of 100% recycled aggregate is non-negligible on the fracture growth though its impact on the global mechanical behavior is not significant.

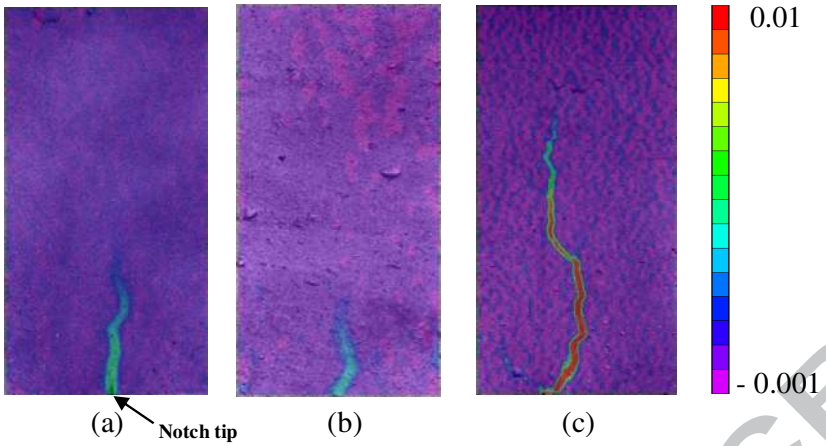

Figure 6: Experimental strain fields (ε_{xx}) for beam (a) C-N-N; (b) C-N-30R; (c) C-N-100R at peak load.

For the purpose of a better understanding of the SLZ evolution, a strip 20 mm long located 5 mm above notch and centered at the cracking zone has been chosen to calculate the strain profile, with consideration to avoid the unstable cracking zone near the notch tip, but to be as close as possible. The results in Figure 7 show that the strain profiles develop with the increasing loading. The strain value is highest at the center of the zone and it reduces gradually towards the edge; a symmetric distribution of the strain value is found.

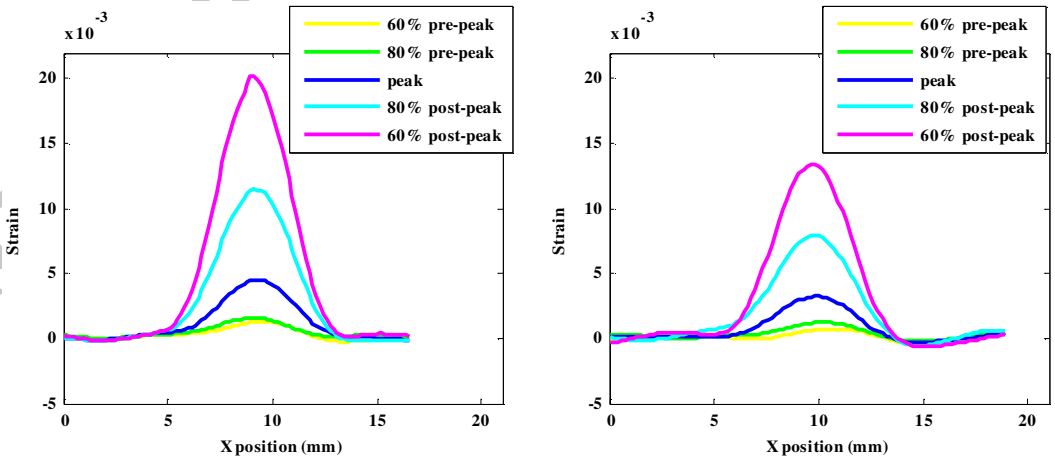

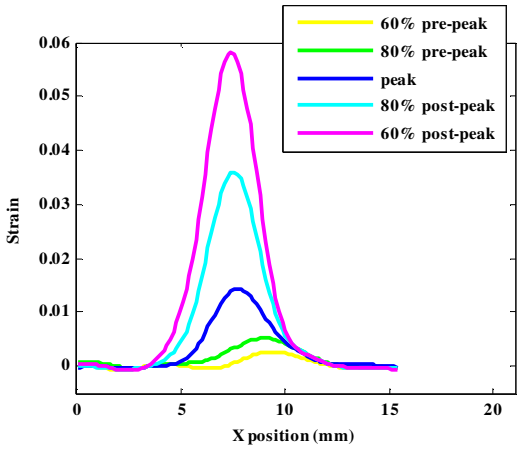

(c)

Figure 7: Experimental strain profiles 5 mm above the notch tip in beams (a) C-N-N; (b) C-N-30R; (c) C-N-100R. Note that for C-N-100R a larger scale is adopted because its strain value is much higher than those of other kinds of concrete.

We observe that with the lowest elastic modulus, C-N-100R has the highest strain value during all loading steps. While for C-N-30R the strain values are lower than those of C-N-N at the same loading step. One possible explanation is that the small percentage of recycled aggregate leads to more diffused local microcracks, which is beneficial for a better local stress relaxation and thus a lower strain value. This suggests that the use of recycled aggregate is not necessarily inauspicious and appropriate result could be achieved.

4.3 Microcracking origin from multi-parametric clustering of AE signals

The mechanical behavior of concrete is governed by initiated defects and their propagation during loading. These localized microcracks can be interpreted by the localization of the acoustic signals. The cumulated AE events throughout the fracture test for specimens C-N-N and C-N-100R are shown in Figure 8. AE events are discretized into six levels of absolute energy (0 – 50 aJ, 50 – 100 aJ, 100 – 300 aJ, 300 –

600 aJ, 600 – 900 aJ and >= 900 aJ). The acoustic activity is assumed to be proportional to the density of the microcracks, which are well distributed across the beam ligament by forming a relatively wide band. It is remarked that compared to normal concrete more events with high energy level are recorded for recycled concrete and their distribution is more intense along the central crack. A detailed discussion on the acoustic localization features for the two kinds of concrete has been presented in Guo et al. [54].

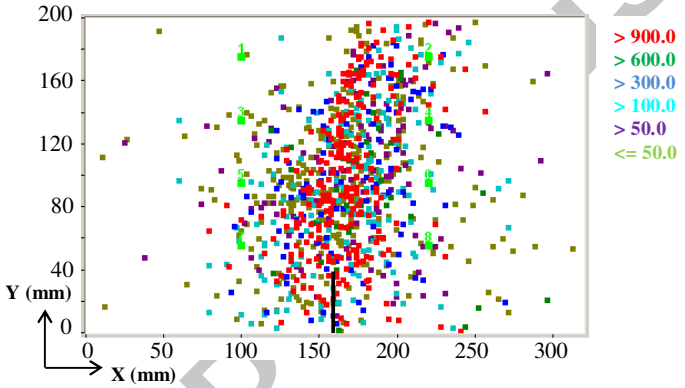

(a)

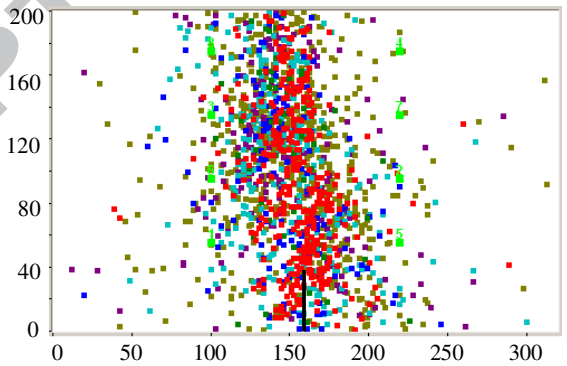

(b)

Figure 8: Localization of the cumulated AE events for (a) C-N-N and (b) C-N-100R.

4.3.1. Cluster identification

Based on a hierarchical dendrogram, the classification of AE data was realized with the non-supervised K-means method that is associated with the principle component analysis (PCA). Six parameters with a correlation level less than 0.95 have been chosen: Rise Time, Counts to Peak, Counts, Duration, Amplitude, Average Frequency and Absolute Energy. In order to impose an equivalent weight factor to each AE component, all the descriptors were normalized in the interval of [-1 1]. Figure 9 presents the results of the K-means method in 2D as function of first and second principle components that represent the most important variance of AE parameters. Three clusters are distinguished for both normal concrete and recycled concrete; the clusters are well separated and discriminated.

For the purpose of knowing more features about the three classes, the amplitude distribution function for each class has been calculated, based on the corresponding normalized number of hits (Figure 10). It is found that the variable of amplitude distribution conforms well to the normal distribution with a probability density function:

$$f(x|\mu,\sigma^2) = \frac{1}{\sqrt{2\pi\sigma^2}} e^{-\frac{(x-\mu)^2}{2\sigma^2}}$$

where x is the studied variable, μ the mean of the distribution and σ the standard deviation. The relevant values and the range of amplitude distribution for the three classes are summarized in Table 5. Note that the classification differences here have to be considered as relative differences and can change with the specimen size and the recording system.

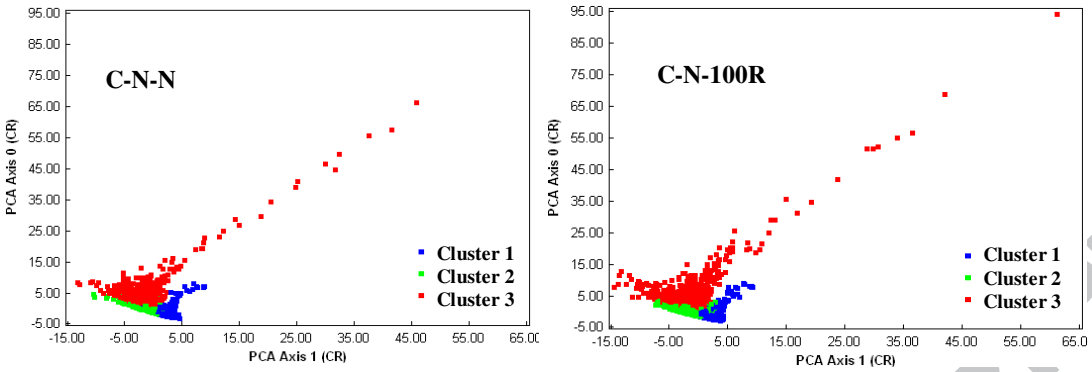

(a) (b)

Figure 9: Visualization of the PCA clusters for (a) C-N-N and (b) C-N-100R.

Table 5: Amplitude distribution characteristics.

	Mean (dB)	Standard deviation (dB)	Amplitude range (dB)
Cluster 1	45.48	4.98	35-55
Cluster 2	43.03	4.17	35-51
Cluster 3	60.76	8.43	40-80

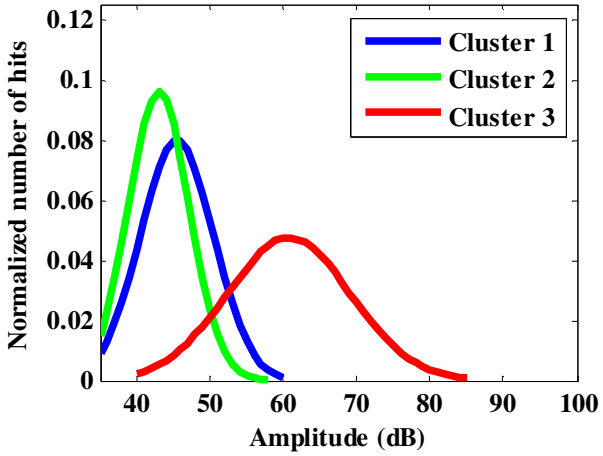

Figure 10: Amplitude distribution for each cluster.

A similar classification is found for C-N-N and C-N-100R. Firstly, the cluster 3 is composed of AE signals with the highest amplitude compared to other clusters. This third class that accounts for more than 95% of the total absolute energy owns the fewest

hit, as shown clearly in Figure 11-12. In addition, there exist the energy jumps for this cluster during the post-peak region and these jumps happen earlier for concrete C-N-100R. Then, with regard to cluster 2, the average amplitude level is much lower than that of cluster 1; the same case is found for the absolute energy. However, the total hit number of this second cluster is the largest, as demonstrated in Figure 12, which means that this group is composed of numerous AE signals with low amplitude and low absolute energy. Moreover, it is noted that for recycled concrete the cumulated absolute energy is higher and the cumulated number of hits is larger by comparison with those of normal concrete. Lastly, for cluster 1, the average amplitude level is between those of the second and the third clusters; the total absolute energy is close to that of the second cluster; the recorded hit number is also between those of the second and the third clusters. For C-N-N, the energy level is relatively lower and the number of hits is smaller compared to C-N-100R.

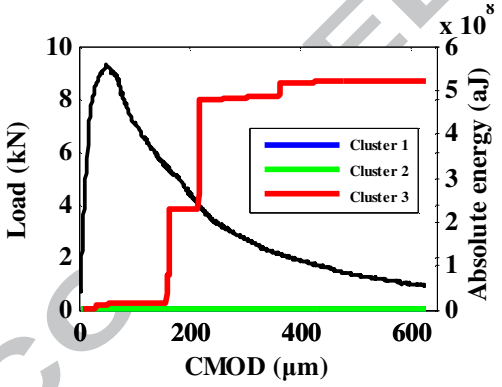

(a)

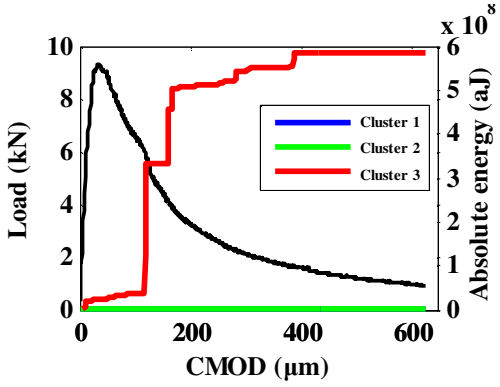

(b)

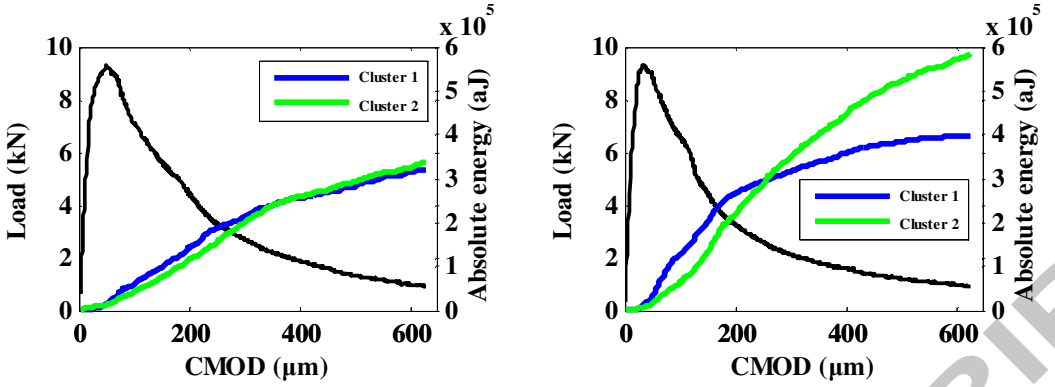

Figure 11: Load-CMOD curve and cumulated absolute energy of each cluster for (a) C-N-N and (b) C-N-100R; zoom of Cluster 1 and Cluster 2 for (c) C-N-N and (d) C-N-100R

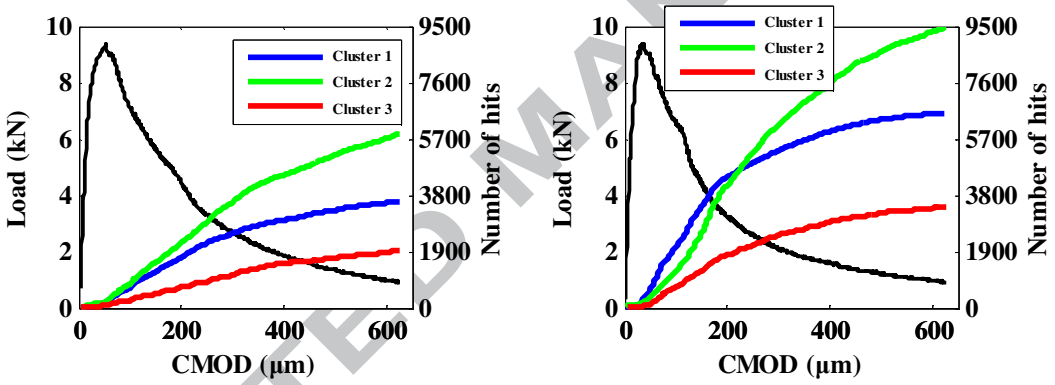

Figure 12: Load-CMOD curve and cumulated hits of each cluster for (a) C-N-N and (b) C-N-100R.

By considering the characteristics of each cluster described above, the third cluster with an amplitude range of 40-80 dB can possibly be attributed to aggregate fracture [55]; the second cluster with an amplitude range of 35-51 dB can possibly be ascribed to microcracking at the ITZ between aggregate and cement mortar [56]; the first cluster with an amplitude range of 35-55 dB can probably be associated to cracking in the cement mortar [55].

4.3.2. Evolution of multi-phase micro-fracture mechanisms in normal and recycled concrete

The apparition chronology of the effective acoustic events for each cluster during the whole test has been analyzed for the two kinds of concrete, as shown in Figure 13-15. We noticed that for cluster 1 (that corresponds to cracking in cement mortar) more events are recorded for recycled concrete though the natural sand is used in this mixture. Microcracks in C-N-N develop in a distributed way along the x position, while for C-N-100R the microcracks localize around the notch. It indicates the reduction of crack meandering during the fracture of recycled concrete. A similar case is found for cluster 2 that corresponds to cracking in ITZ, which can be explained by the fact that two kinds of transition zone exist in RAC, one between the recycled aggregate and new mortar and the other between the recycled aggregate and the old attached mortar. These phenomena confirm the complicated microstructure of RAC. Concerning the third cluster that corresponds to aggregate fracture, more signals are captured during the failure of C-N-100R and they are located intensely near the notch. One possible explanation is that the recycled aggregate with low particle strength tends to crush under loading while the natural aggregate remain mostly intact. Consequently, the cracks in recycled concrete develop more easily and faster compared to normal concrete. However, it should be admitted that clusters 1 and 2 possibly contain the AE signals that are due to the crack-face friction, crack branching, aggregate bridging and other toughening mechanisms.

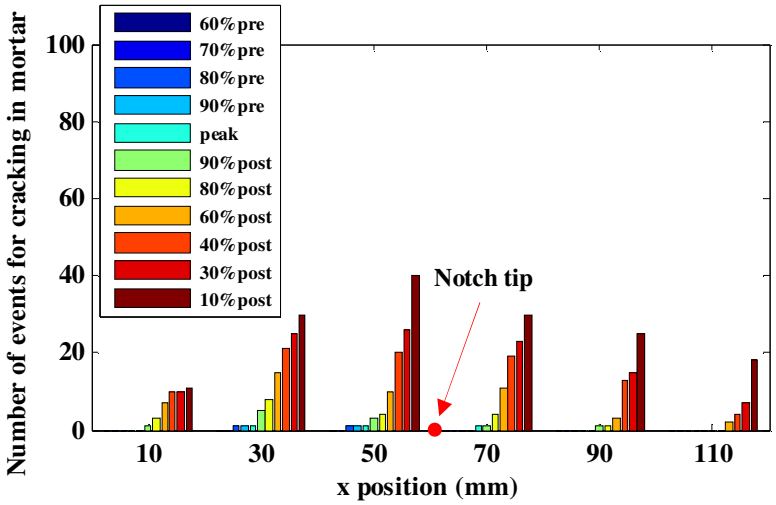

(a)

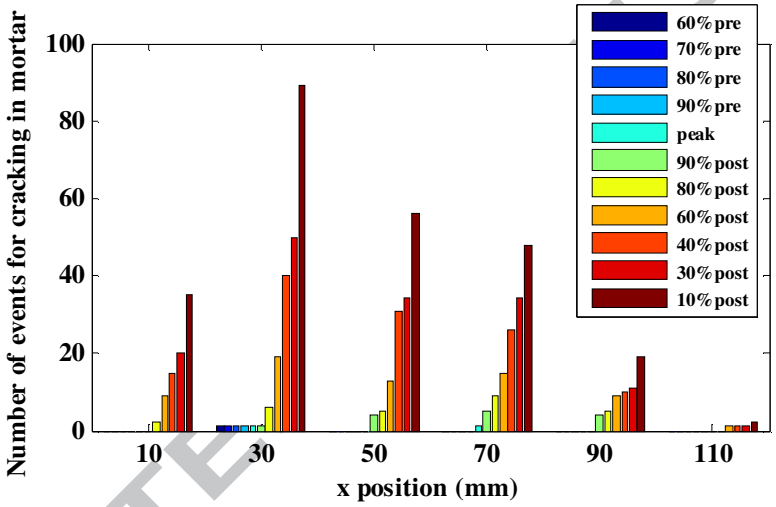

(b)

Figure 13: Apparition chronology of events for cracking in cement mortar (a) C-N-N and (b) C-N-100R.

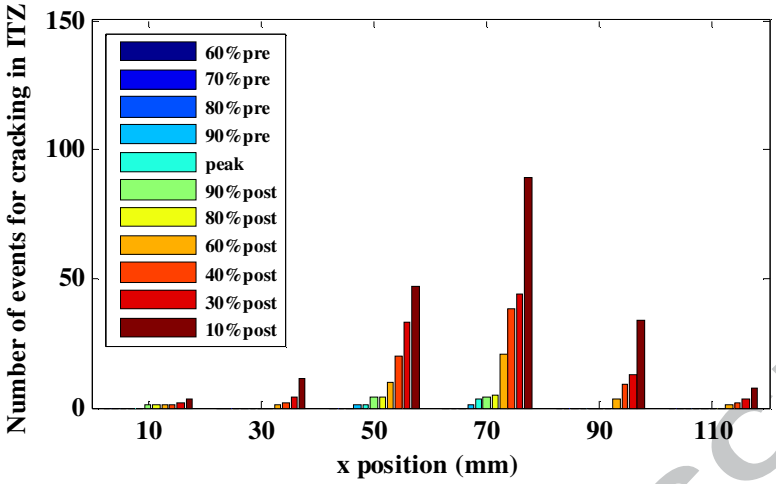

(a)

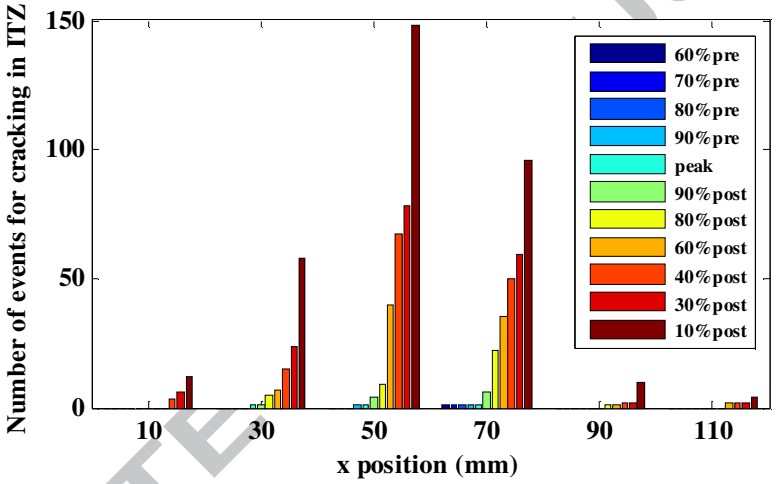

(b)

Figure 14: Apparition chronology of events for cracking in ITZ (a) C-N-N and (b) C-N-100R.

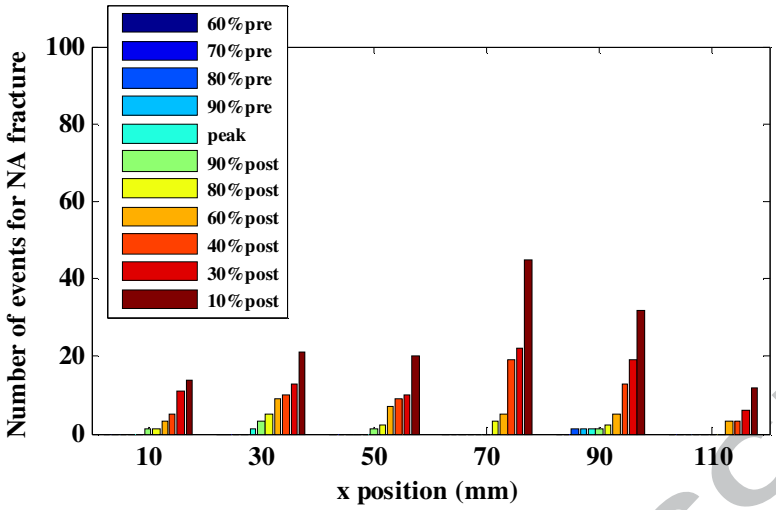

(a)

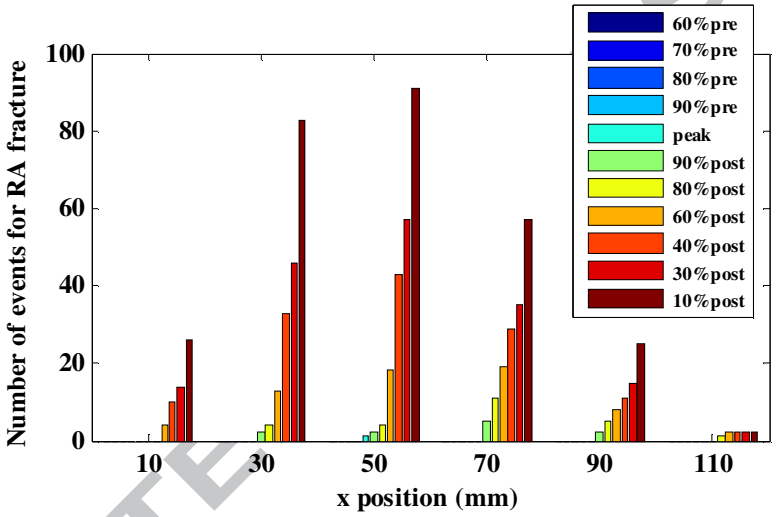

(b)

Figure 15: Apparition chronology of events for aggregate fracture (a) C-N-N and (b) C-N-100R (NA: Natural Aggregate and RA: Recycled Aggregate).

5. General remarks on results

The fracture behavior of recycled aggregate concrete has been compared with normal aggregate concrete. The results clearly indicate that 100% replacement by recycled aggregate significantly increases the risk of cracking. Therefore the complete replacement should be avoided in the construction of structures using recycled aggregate concrete. Small portion of recycled aggregate up to 30% of total aggregate

content can be used and no significant effect on the fracture properties and fracture mechanisms has been observed. The increase of recycled aggregate content mainly affects the fracture growth and reduces the safe loading limits before cracking.

The recycled aggregate used in our study is obtained by crushing the mix of unknown waste concrete and is provided by one of the largest French recycling platforms (DLB de Gonesse) and the source concrete came from the surrounding demolition sites. Therefore, the recycled materials used in this study represent the properties of various collected waste in general construction and demolition sites. Normally, similar results should be found if we use recycled aggregate from other construction and demolition waste.

6. Conclusion

A comprehensive analysis on the fracture process of recycled concrete has been performed and compared with that of the normal concrete of the same structural class. The aim was to differentiate the micro-fracture mechanisms through quantitative measurements of the key fracture parameters. Following conclusions can be drawn:

- Besides the similar global mechanical behavior (observed in the flexural tests), the characteristic properties such as compressive strength, tensile strength, elastic modulus and fracture energy decrease with the increase of recycled aggregate content. It indicates that the local fracture mechanisms alter due to presence of recycled aggregate. Similar conclusion has also been found in [9]; [11]; [12]; [13].
- In recycled aggregate concrete, crack opening starts at a lower loading step (60% pre-peak in C-N-100R and 70% pre-peak in C-N-30R) as compared to normal aggregate concrete (80% pre-peak). Moreover, the crack development is faster in recycled aggregate concrete (fracture length of C-N-100R is two times

than that of C-N-N). It shows that the risk of cracking in recycled aggregate concrete is more under service loadings. Moreover, faster crack development in such concrete may lead to catastrophic failures.

- Higher strain gradients are observed in the localized damage zone in recycled aggregate concrete. It is due to strong discontinuities or existing cracks in recycled aggregate which helps in localization of the main crack. Since fracture is observed at the interface between aggregate and mortar, the higher strain gradient and low stiffness of the recycled aggregate concrete also indicates the weak interface between the new mortar and recycled aggregate which is supposedly due to high porosity and existing cracks.
- By applying acoustic emission classification method, three clusters with different AE features are discriminated for both normal and recycled concrete. The specific characteristics of each cluster helps assigning each cluster to a certain micro-fracture phenomenon occurring during the failure process. It can be concluded that in case of recycled aggregate concrete, the leading micro-fracture phenomenon is ITZ cracking. Also the micro-fractures (all phases) are more localized and intense as compared to normal concrete. It indicates a weak bond between mortar and recycled aggregate which would be the principal cause of failure of recycled concrete structures.

The detailed description of the failure process presented in this paper can provide the information for improving the durability and service life of RAC structures. As the material failure at the structural scale usually starts by the formation and growth of local microcracks, the quantitative analysis of the cracking process of laboratory specimens contributes to the understanding of the failure behavior of engineering recycled concrete structures. Moreover, the obtained mechanical properties can be used as the benchmark

parameters for the modeling of recycled concrete structures. In order to go further in the understanding of microstructural damage mechanism of recycled aggregate concrete, mortar specimen should be tested and monitored with AE technique and the corresponding results will complement to a better classification of failure mechanisms in recycled aggregate concrete. Based on the experimental results presented in this work, authors have also done multiscale numerical modeling to take into account the effect of the complex microstructure on the fracture process of recycled concrete. A paper on this part is under progress which will be submitted very soon.

Acknowledgments

This study has been performed in the project ECOREB which is supported by the French National Research Agency (ANR: Agence Nationale pour la Recherche) in the program " Villes et batiments Durables" (sustainable cities and buildings).

References

[1] NF EN 206/CN, "Béton-Spécification, performance, production et confirmité-Complément national à la norme NF EN 206," 2014.

[2] V. W. Y. Tam, X. F. Gao, and C. M. Tam, "Microstructural analysis of recycled aggregate concrete produced from two-stage mixing approach," *Cem. Concr. Res.*, vol. 35, pp. 1195–1203, 2005.

[3] M. Etxeberria, E. Vazquez, and A. Mari, "Microstructure analysis of hardened recycled aggregate concrete," *Mag. Concr. Res.*, vol. 58, pp. 683–690, 2006.

[4] Z. Zhao, S. Remond, D. Damidot, and W. Xu, "Influence of fine recycled concrete aggregates on the properties of mortars," *Constr. Build. Mater.*, vol. 81, pp. 179–186, 2015.

[5] K. H. Yang, H. S. Chung, and A. F. Ashour, "Influence of type and replacement level of recycled aggregates on concrete properties," *ACI Mater. J.*, vol. 105, no. 105, pp. 289–296, 2008.

[6] L. Evangelista and J. de Brito, "Durability performance of concrete made with fine recycled concrete aggregates," *Cem. Concr. Compos.*, vol. 32, no. 1, pp. 9–14, 2010.

[7] A. Z. Bendimerad, E. Roziere, and A. Loukili, "Combined experimental methods to assess absorption rate of natural and recycled aggregates," *Mater. Struct.*, vol. 48, no. 11, pp. 3557–3569, Nov. 2015.

[8] M. Casuccio, M. C. Torrijos, G. Giaccio, and R. Zerbino, "Failure mechanism of recycled aggregate concrete," *Constr. Build. Mater.*, vol. 22, pp. 1500–1506, 2008.

[9] C. S. Poon, Z. H. Shui, and L. Lam, "Effect of microstructure of ITZ on compressive strength of concrete prepared with recycled aggregates," *Constr. Build. Mater.*, vol. 18, pp. 461–468, 2004.

[10] J. Xiao, W. Li, Z. Sun, D. A. Lange, and S. P. Shah, "Properties of interfacial transition zones in recycled aggregate concrete tested by nanoindentation," *Cem. Concr. Compos.*, vol. 37, pp. 276–292, 2013.

[11] Q. Liu, J. Xiao, and Z. Sun, "Experimental study on the failure mechanism of recycled concrete," *Cem. Concr. Res.*, vol. 41, no. 10, pp. 1050–1057, 2011.

[12] S. C. Kou, C. S. Poon, and M. Etxeberria, "Influence of recycled aggregates on long term mechanical properties and pore size distribution of concrete," *Cem. Concr. Compos.*, vol. 33, no. 2, pp. 286–291, 2011.

[13] J. R. Roesler, V. Cervantes, and A. Bordelon, "Fracture properties of concrete containing recycled concrete aggregates," *Mag. Concr. Res.*, vol. 61, pp. 665–670, 2009.

[14] J. Xiao, W. Li, Y. Fan, and X. Huang, "An overview of study on recycled aggregate concrete in China (1996-2011)," *Constr. Build. Mater.*, vol. 31, pp. 364–383, 2012.

[15] K. H. Yang, H. S. Chung, and A. F. Ashour, "Influence of type and replacement level of recycled aggregates on concrete properties," *ACI Mater. J.*, vol. 105, pp. 289–296, 2008.

[16] G. Wardeh, E. Ghorbel, and H. Gomart, "Mix Design and Properties of Recycled Aggregate Concretes: Applicability of Eurocode 2," *Int. J. Concr. Struct. Mater.*, vol. 9, no. 1, pp. 1–20, Mar. 2015.

[17] G.-F. Belén, M.-A. Fernando, C. L. Diego, and S.-P. Sindy, "Stress–strain relationship in axial compression for concrete using recycled saturated coarse aggregate," *Constr. Build. Mater.*, vol. 25, pp. 2335–2342, 2011.

[18] S. P. Shah, S. E. Swartz, and C. Ouyang, *Fracture mechanics of concrete: applications of fracture mechanics to concrete, rock and other quasi-brittle materials*. New York: Wiley, 1995.

[19] Z. P. Bažant and J. Planas, *Fracture and size effect in concrete and other quasibrittle materials*. CRC Press, 1998.

[20] S. Y. Alam, J. Saliba, and A. Loukili, "Fracture examination in concrete through combined digital image correlation and acoustic emission techniques," *Constr. Build. Mater.*, vol. 69, pp. 232–242, 2014.

[21] A. Hillerborg, M. Modéer, and P.-E. Petersson, "Analysis of crack formation and crack growth in concrete by means of fracture mechanics and finite elements," *Cem. Concr. Res.*, vol. 6, pp. 773–781, 1976.

[22] H. Nakamura and T. Higai, "Compressive fracture energy and fracture zone length of concrete," *Model. Inelast. Behav. RC Struct. under Seism. Loads, ASCE*, pp. 471–487, 2001.

[23] W. Li, J. Xiao, Z. Sun, and S. P. Shah, "Failure processes of modeled recycled aggregate concrete under uniaxial compression," *Cem. Concr. Compos.*, vol. 34, pp. 1149–1158, 2012.

[24] Ł. Skarżyński, E. Syroka, and J. Tejchman, "Measurements and Calculations of the Width of the Fracture Process Zones on the Surface of Notched Concrete Beams," *Strain*, vol. 47, no. s1, pp. e319–e332, Jun. 2011.

[25] G. K. Kocur, E. H. Saenger, and T. Vogel, "Elastic wave propagation in a segmented X-ray computed tomography model of a concrete specimen," *Constr. Build. Mater.*, vol. 24, no. 12, pp. 2393–2400, 2010.

[26] B. Hilloulin *et al.*, "Small crack detection in cementitious materials using nonlinear coda wave modulation," *NDT E Int.*, vol. 68, pp. 98–104, 2014.

[27] H. Mihashi, N. Nomura, and S. Niiseki, "Influence of aggregate size on fracture process zone of concrete detected with three dimensional acoustic emission technique," *Cem. Concr. Res.*, vol. 21, no. 5, pp. 737–744, Sep. 1991.

[28] K. Otsuka and H. Date, "Fracture process zone in concrete tension specimen," *Eng. Fract. Mech.*, vol. 65, no. 2–3, pp. 111–131, Jan. 2000.

[29] K. Haidar, G. Pijaudier-Cabot, J. F. Dubé, and A. Loukili, "Correlation between the internal length, the fracture process zone and size effect in model materials," *Mater. Struct.*, vol. 38, no. 2, pp. 201–210, Mar. 2005.

[30] C. Grosse and M. Ohtsu, *Acoustic emission testing in engineering: basics and applications*. Berlin: Springer, 2008.

[31] D. Grégoire *et al.*, "Mesoscale analysis of failure in quasi-brittle materials: comparison between lattice model and acoustic emission data," *Int. J. Numer. Anal. Methods Geomech.*, vol. 39, no. 15, pp. 1639–1664, Oct. 2015.

[32] B. L. Karihaloo, A. R. Murthy, and N. R. Iyer, "Determination of size-independent specific fracture energy of concrete mixes by the tri-linear model," *Cem. Concr. Res.*, vol. 49, pp. 82–88, Jul. 2013.

[33] E. N. Landis and L. Baillon, "Experiments to Relate Acoustic Emission Energy to Fracture Energy of Concrete," *J. Eng. Mech.*, vol. 128, no. 6, pp. 698–702, Jun. 2002.

[34] S. Muralidhara, B. K. R. Prasad, H. Eskandari, and B. L. Karihaloo, "Fracture process zone size and true fracture energy of concrete using acoustic emission," *Constr. Build. Mater.*, vol. 24, no. 4, pp. 479–486, Apr. 2010.

[35] K. Ohno and M. Ohtsu, "Crack classification in concrete based on acoustic emission," *Constr. Build. Mater.*, vol. 24, no. 12, pp. 2339–2346, Dec. 2010.

[36] D. G. Aggelis, "Classification of cracking mode in concrete by acoustic emission parameters," *Mech. Res. Commun.*, vol. 38, no. 3, pp. 153–157, Apr. 2011.

[37] [37] S. Y. Alam and A. Loukili, "Transition from energy dissipation to crack openings during continuum – discontinuum fracture of concrete," Int. J. Fracture, vol 206, no. 1, pp 49–66, July 2017.

[38] Ł. Skarżyński and J. Tejchman, "Calculations of fracture process zones on meso-scale in notched concrete beams subjected to three-point bending," *Eur. J. Mech. - A/Solids*, vol. 29, no. 4, pp. 746–760, Jul. 2010.

[39] Z. Wu, H. Rong, J. Zheng, F. Xu, and W. Dong, "An experimental investigation on the FPZ properties in concrete using digital image correlation technique," *Eng. Fract. Mech.*, vol. 78, no. 17, pp. 2978–2990, Dec. 2011.

[40] S. Y. Alam, A. Loukili, and F. Grondin, "Monitoring size effect on crack opening in concrete by digital image correlation," *Eur. J. Environ. Civ. Eng.*, vol. 16, no. 7, pp. 818–836, 2012.

[41] S. Y. Alam, P. Kotronis, and A. Loukili, "Crack propagation and size effect in concrete using a non-local damage model," *Eng. Fract. Mech.*, vol. 109, pp. 246–261, 2013.

[42] J. Réthoré, F. Hild, and S. Roux, "Extended digital image correlation with crack shape optimization," *Int. J. Numer. Methods Eng.*, vol. 73, no. 2, pp. 248–272, Jan. 2008.

[43] "PN-RECYBETON, RECYBETON: RECYclage complet des BETONs," France, 2011. http://www.pnrecybeton.fr/

[44] "Projet ANR ECOREB, ECOREB: ECOconstruction par le REcyclage du Béton," France, 2012. http://www.agence-nationale-recherche.fr/?Projet=ANR-12-VBDU-0003

[45] S. Omary, E. Ghorbel, and G. Wardeh, "Relationships between recycled concrete aggregates characteristics and recycled aggregates concretes properties," *Constr. Build. Mater.*, vol. 108, pp. 163–174, 2016.

[46] A. Z. Bendimerad, E. Rozière, and A. Loukili, "Plastic shrinkage and cracking risk of recycled aggregates concrete," *Constr. Build. Mater.*, vol. 121, pp. 733–745, 2016.

[47] F. De Larrard and T. Sedran, "Le logiciel BetonlabPro 3: Bulletin des laboratoires des ponts et chaussées." p. BLPC no.270–271, In French, 2007.

[48] Eurocode 2, "Design of concrete structures," no. EN 1992-1-1.

[49] A. Hillerborg, "The theoretical basis of a method to determine the fracture energy GF of concrete," *Mater. Struct.*, vol. 18, pp. 291–296, 1985.

[50] RILEM TCS, "Determination of the fracture energy of mortar and concrete by means of three-point bend tests on notched beams," *Mater. Struct.*, vol. 18, no. 106, pp. 285–290, 1985.

[51] B. L. Karihaloo, "A new philosophy for the design of RC structures based on concepts of fracture mechanics," *Procedia Mater. Sci.*, vol. 3, no. 0, pp. 369–377, 2014.

[52] Mindess S., "Fracture process zone detection," in *Report RILEM TC 89-FMT: Fracture Mechanics Test-Methods for Concrete*, S. P. Shah and A. Carpinteri, Eds. London/New york: Chapman & Hall, 1991, pp. 231–261.

[53] K. Wang, D. C. Jansen, and S. P. Shah, "Permeability Study of Cracked Concrete," *Cem. Concr. Res.*, vol. 27, no. 3, pp. 381–393, 1997.

[54] M. Guo, F. Grondin, S. Y. Alam, and A. Loukili, "Fracture process analysis of recycled aggregate concrete with combined acoustic emission and digital image correlation techniques," in *9th International Conference on Fracture Mechanics of Concrete and Concrete Structures*, 2016.

[55] K. Wu, B. Chen, and W. Yao, "Study on the AE characteristics of fracture process of mortar, concrete and steel-fiber-reinforced concrete beams," *Cem. Concr. Res.*, vol. 30, no. 9, pp. 1495–1500, 2000.

[56] J. Saliba, A. Loukili, F. Grondin, and J. P. Regoin, "Identification of damage mechanisms in concrete under high level creep by the acoustic emission technique," *Mater. Struct.*, vol. 47, pp. 1041–1053, 2013.

Highlights

- The distinctive fracture characteristics of normal and recycled concrete were analyzed.
- Different damage mechanisms of recycled concrete were identified.
- The quantitative analysis of the micro-fracture in each phase of the recycled concrete was carried out.
- The evolution of each kind of micro-fracture in function of the loading step was demonstrated.